Eur. Phys. J. Special Topics **227**, 1077–1090 (2018)

https://doi.org/10.1140/epjst/e2018-800084-6

THE EUROPEAN PHYSICAL JOURNAL SPECIAL TOPICS

Regular Article

Noise-induced switching in two adaptively coupled excitable systems

Iva Bačić[1], Serhiy Yanchuk[2], Matthias Wolfrum[3], and Igor Franović[1,a]

[1] Scientific Computing Laboratory, Center for the Study of Complex Systems, Institute of Physics Belgrade, University of Belgrade, Pregrevica 118, 11080 Belgrade, Serbia
[2] Institute of Mathematics, Technische Universität Berlin, Straße des 17. Juni 136, 10623 Berlin, Germany
[3] Weierstrass Institute, Mohrenstrasse 39, 10117 Berlin, Germany

Received 30 April 2018 / Received in final form 19 June 2018
Published online 12 December 2018

Abstract. We demonstrate that the interplay of noise and plasticity gives rise to slow stochastic fluctuations in a system of two adaptively coupled active rotators with excitable local dynamics. Depending on the adaptation rate, two qualitatively different types of switching behavior are observed. For slower adaptation, one finds alternation between two modes of noise-induced oscillations, whereby the modes are distinguished by the different order of spiking between the units. In case of faster adaptation, the system switches between the metastable states derived from coexisting attractors of the corresponding deterministic system, whereby the phases exhibit a bursting-like behavior. The qualitative features of the switching dynamics are analyzed within the framework of fast-slow analysis.

1 Introduction

In many complex systems, ranging from biology, physics and chemistry to social sciences and engineering, the interaction patterns are not static, but are rather affected by the states of constituent units [1–4]. This gives rise to complex feedback mechanisms, where the coupling weights adapt to dynamical processes at the units, which in turn influences the evolution of units itself. Modeling of such systems is based on the paradigm of adaptive networks, where self-organization unfolds both at the level of coupling weights and the collective states of the units, typically involving a separation of characteristic timescales. The faster and the slower timescales are naturally associated to the dynamics of units and couplings, respectively, such that the short-term evolution of the units occurs on a quasi-static network, whereas the slow changes in coupling weights depend on the time-averaged dynamics of the units. An important example of adaptive connectivity is provided by neuronal systems, where the strength of synaptic couplings is adjusted to the underlying spiking activity via spike-time-dependent plasticity (STDP), a temporally asymmetric form of Hebbian learning [5],

[a] e-mail: franovic@ipb.ac.rs

promoting causal relationship between the spikes of pre- and postsynaptic neurons [6–8].

Motivated by the research on neuronal systems, in the present paper we study a simplified model which incorporates the basic ingredients of neurodynamics, such as excitability, plasticity and noise. The considered system consists of two adaptively coupled active rotators, whose intrinsic dynamics is set to excitable regime and subjected to noise. The plasticity rule is introduced in such a way that one may continuously interpolate between the coupling dynamics characteristic to Hebbian learning and STDP. We demonstrate that the interplay of plasticity and noise may facilitate two qualitatively different forms of slow stochastic fluctuations, depending on the adaptation rate. While for slower adaptation the self-organized dynamics consists of switching between the two modes of noise-induced oscillations, in case of faster adaptation, the switching dynamics comprises metastable states associated to attractors of the deterministic system.

In the context of neuroscience, one may compare the considered system to a binary neuron motif. It is well known that the same structural motif, defined at the level of anatomy, can support multiple functional motifs [9–12], characterized by different weight configurations and potentially distinct directions of information flow. In these terms, our study will show that the co-effect of plasticity and noise may (i) contribute to the emergence of different functional motifs on top of the given structural one and (ii) trigger slow alternation between the functional motifs.

So far, the co-effects of noise and the STDP plasticity rule have been analyzed in systems of two coupled neural oscillators, as well as in networks of oscillators. In case of two units, multistability between different weight configurations has been found, surprisingly indicating that noise may stabilize configurations of strong bidirectional coupling absent in the deterministic system [13]. At variance with this, our study concerns excitable local dynamics and explicitly addresses the slow stochastic fluctuations between metastable states. For networks of adaptively coupled neural or phase oscillators, the previous research has mainly focused on the impact of plasticity on the synchronization behavior. In the absence of noise, several generic forms of macroscopic dynamics have been identified, including desynchronized or partially synchronized states with weak couplings, as well as cluster states [14–18]. In presence of noise, an interesting effect of self-organized noise resistance to desynchronization has been reported in the case of a network of neural oscillators [19]. In networks of excitable units, the STDP rule has been shown to give rise to oscillating coupling configurations that facilitate switching between strongly and weakly synchronized states [20–22].

The paper is organized as follows. The details of the model are introduced in Section 2. An overview of the underlying deterministic dynamics, characterizing the impact of plasticity on the stationary states and the onset of emergent oscillations, is provided in Section 3. Section 4 is dedicated to a fast–slow analysis of the deterministic dynamics, whereas in Section 5 are explained the features of the two generic types of switching behavior. In Section 6 we provide a summary of our main results.

2 Model

We consider a system of two stochastic active rotators interacting by adaptive couplings, where the dynamics of the phases $\{\varphi_1(t), \varphi_2(t)\}$ and the coupling weights $\{\kappa_1(t), \kappa_2(t)\}$ is given by

$$\begin{aligned}
\dot{\varphi_1} &= I_0 - \sin\varphi_1 + \kappa_1 \sin(\varphi_2 - \varphi_1) + \sqrt{D}\xi_1 \\
\dot{\varphi_2} &= I_0 - \sin\varphi_2 + \kappa_2 \sin(\varphi_1 - \varphi_2) + \sqrt{D}\xi_2 \\
\dot{\kappa_1} &= \epsilon(-\kappa_1 + \sin(\varphi_2 - \varphi_1 + \beta)) \\
\dot{\kappa_2} &= \epsilon(-\kappa_2 + \sin(\varphi_1 - \varphi_2 + \beta)),
\end{aligned} \tag{1}$$

where $\varphi_1, \varphi_2 \in S^1$, while κ_1 and κ_2 are real variables. The rotators are assumed to be identical, having their local dynamics governed by the excitability parameter I_0, which gives rise to a SNIPER bifurcation at $I_0 = 1$. We focus on the excitable regime, such that $I_0 = 0.95$ is kept fixed throughout the paper. In this case, the uncoupled system always converges to a steady state, whereas the collective dynamics emerges due to interaction and noise. The parameter $\epsilon \ll 1$ defines the scale separation between the fast dynamics of the phases and the slow dynamics of adaptation. White noise of variance D acts only within the subspace of fast variables, whereby the terms $\xi_1(t)$ and $\xi_2(t)$ are independent ($\xi_i(t)\xi_j(t') = \delta_{ij}\delta(t-t')$ for $i, j \in \{1, 2\}$). In the context of neuroscience, I_0 can be interpreted as external bias current, whereas the impact of stochastic terms is analogous to that of synaptic noise. Note that the deterministic version of (1) is symmetric with respect to the exchange of indices $1 \leftrightarrow 2$.

The plasticity rule is controlled by the parameter β, which allows one to interpolate between the different adaptation modalities. The analogy between the adaptivity dynamics in classical neuronal systems and the systems of coupled phase oscillators has been addressed in [14,23,24], whereas a deeper analysis of the correspondence between the phase-dependent plasticity rules and the STDP has been provided in [13]. From these studies, it follows that the scenario found for $\beta = 3\pi/2$, where the stationary weights increase for smaller phase differences and decrease for larger ones ("like-and-like" form of behavior), qualitatively resembles the Hebbian learning rule [23,24]. Nevertheless, in the case $\beta = \pi$, the two coupling weights always change in opposite directions, which may be interpreted as promoting an STDP-like plasticity rule. In the present paper, we are interested in the β interval between these two limit cases, since it admits two coexisting excitable fixed points.

3 Deterministic dynamics of the full system

In this section, we analyze the details of the *deterministic* dynamics of the full system (1), considering first the stationary states and the associated excitability feature, and then focusing on the scenario that gives rise to emergent oscillations.

3.1 Stationary states and excitable dynamics

Fixed points $(\varphi_1^*, \varphi_2^*, \kappa_1^*, \kappa_2^*)$ of the complete system (1) for $D = 0$ are given by the solutions of the following set of equations:

$$\begin{aligned} \sin\varphi_1^* - \sin(\varphi_2^* - \varphi_1^* + \beta)\sin(\varphi_2^* - \varphi_1^*) &= I_0, \\ \sin\varphi_2^* - \sin(\varphi_1^* - \varphi_2^* + \beta)\sin(\varphi_1^* - \varphi_2^*) &= I_0, \end{aligned} \tag{2}$$

with

$$\begin{aligned} \kappa_1^* &= \sin(\varphi_2^* - \varphi_1^* + \beta), \\ \kappa_2^* &= \sin(\varphi_1^* - \varphi_2^* + \beta). \end{aligned} \tag{3}$$

Equation (2) can be solved numerically for any fixed parameter set, or numerical path-following can be applied in order to study the dependence of the fixed points on the parameters.

The bifurcation diagram in Figure 1 shows how the number and stability of fixed points of the full system change with β. In particular, depending on β, there may be two, four or six fixed points. Due to symmetry, the solutions always appear in pairs of points sharing the same stability features. Since our study concerns plasticity rules which support excitable fixed points, we have confined the analysis to the interval $\beta \in (3.298, 4.495)$, where the system has *two stable* fixed points, which lie off the synchronization manifold $\varphi_1 = \varphi_2$. Apart from that, there are also four unstable

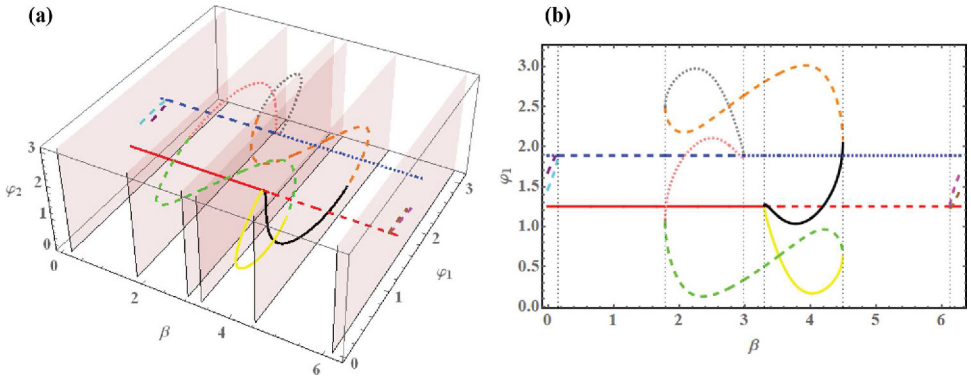

Fig. 1. (a) Bifurcation diagram for the fixed points of system (1) with $D = 0$ in the $(\beta, \varphi_1, \varphi_2)$ space. (b) Projection of the bifurcation diagram to (β, φ_1) plane. The two fixed points independent on β belong to the synchronization manifold: the red (blue) one is always longitudinally stable (unstable). The solid lines denote stable fixed points, whereas the dashed and dotted lines denote saddles of unstable dimension 1 and 2, respectively.

fixed points. The bifurcations associated to the boundaries of the given β interval are as follows: at $\beta = 3.298$ the system undergoes a supercritical symmetry-breaking pitchfork bifurcation where a symmetry related pair of two stable fixed points off the synchronization manifold is created, whereas at $\beta = 4.495$, this pair meets another pair of unstable fixed points off the synchronization manifold such that both are annihilated in symmetry related inverse saddle-node bifurcations. For instance, at $\beta = 4.1$, one finds the symmetry related pair of stable foci given by $(\varphi_1, \varphi_2, \kappa_1, \kappa_2) = (1.177, 0.175, 0.032, -0.92)$ and $(\varphi_1, \varphi_2, \kappa_1, \kappa_2) = (0.175, 1.177, -0.92, 0.032)$. Note that these weight levels support effective master-slave configurations, where one unit exerts a much stronger influence on the other unit than vice versa.

The two stable asymmetric fixed points in the interval $\beta \in (3.298, 4.495)$ are excitable, and may exhibit several different types of response to external perturbations, see the classification in Figure 2. Introducing the perturbations by setting different initial conditions, we plot in Figure 2 the phase dynamics in the fast subspace while keeping the weights (κ_1, κ_2) fixed. Note that in the case where both units respond with a single spike, the order of firing is such that the unit with larger initial phase $\varphi_i(0), i \in \{1, 2\}$ fires first.

3.2 Onset of oscillations

The onset of emergent oscillations in system (1) with $D = 0$ depends on the interplay between the plasticity rule, specified by β, and the speed of adaptation, characterized by ϵ. A parameter scan indicating the variation of κ_1, $A_{\kappa_1} = \max(\kappa_1(t)) - \min(\kappa_1(t))$ in terms of (β, ϵ) is shown in Figure 3a. The results are obtained by numerical continuation beginning from a stable periodic solution, such that the final state reached for a certain set of (β, ϵ) values provides the initial conditions for the simulation of the system at incremented parameter values. By this method, we have determined the maximal stability region of the periodic solution.

One finds that for a fixed β, there actually exists an interval of timescales separation $\epsilon \in (\epsilon_{min}, \epsilon_{max})$ admitting oscillations, cf. Figure 3b. The periodic solutions in this interval coexist with the two symmetry-related stable stationary states. One observes that the threshold ϵ_{min} reduces with β, whereas the upper boundary value ϵ_{max} grows with increasing β. The detailed bifurcation mechanisms behind the onset

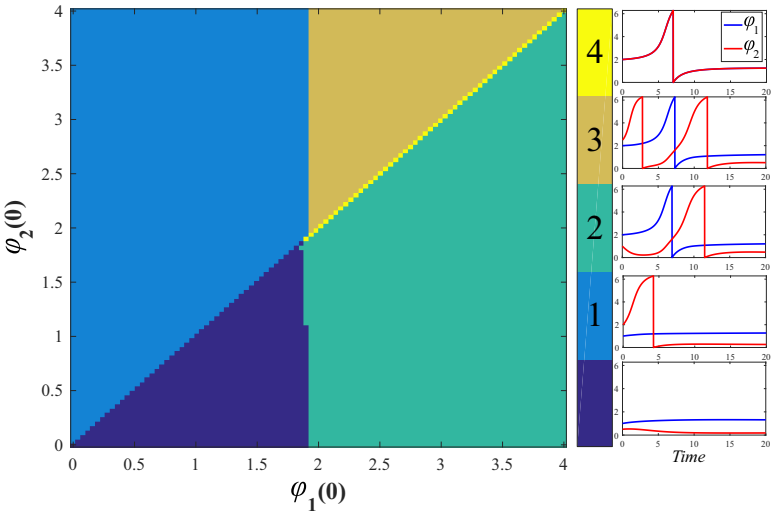

Fig. 2. Modalities of the response to external perturbation for system (1) with $D = 0$. The system parameters are $I_0 = 0.95$, $\epsilon = 0.01$ and $\beta = 4.212$, whereas the initial conditions for the coupling weights are set to $\kappa_1(0) = -0.0077$, $\kappa_2(0) = -0.846$. Depending on the initial phases $(\varphi_1(0), \varphi_2(0))$, one may observe the following regimes: (0) no spikes; (1) the unit with larger $\varphi(0)$ emits one spike and the other does not; (2) both units emit a single spike, with the unit with larger $\varphi(0)$ firing first; (3) the unit with larger $\varphi(0)$ emits two spikes and the other unit emits one; (4) both units spike synchronously.

of oscillations and multistability are beyond the scope of this paper, and essentially involve an interplay between the fast and slow variables.

Enhancing ϵ under fixed β gives rise to a supercritical symmetry-breaking pitchfork bifurcation of limit cycles, indicated by PFL in Figure 3b. Below the bifurcation, the phases $\varphi_1(t)$ and $\varphi_2(t)$ maintain a small phase-shift, while the oscillation profiles $\kappa_i(t), i \in \{1, 2\}$ are rather different, see Figures 3d and 3e, respectively. Above the bifurcation, the system gains the anti-phase space-time symmetry $\varphi_1(t) = \varphi_2(t + T/2), \kappa_1(t) = \kappa_2(t + T/2)$ where T denotes the oscillation period, cf. the associated waveforms in Figures 3g and 3f.

4 Slow-fast analysis of the deterministic dynamics

The deterministic dynamics in case of slow adaptation, corresponding to a strong timescale separation between the fast and slow variables, may be analyzed within the framework of standard fast-slow analysis. In general, one may either consider the layer problem, defined on the fast timescale, or the reduced problem, which concerns the slow timescale. Within the layer problem, the aim is to determine the fast flow dynamics $\varphi_1(t; \kappa_1, \kappa_2), \varphi_2(t; \kappa_1, \kappa_2)$ by treating the slow variables κ_1 and κ_2 as parameters, whereas the reduced problem consists in determining the dynamics of the slow flow $(\kappa_1(t), \kappa_2(t))$ (reduced flow) assuming that the fast flow of the layer problem is either at a stable equilibrium or at the averaged value of a stable regime.

In this section, we first investigate the fast layer problems. Depending on the values of the slow variables (κ_1, κ_2), the fast flow can exhibit several attractors, such that multiple sheets of the slow flow emerge from the averaged dynamics on the different attractors of the fast flow.

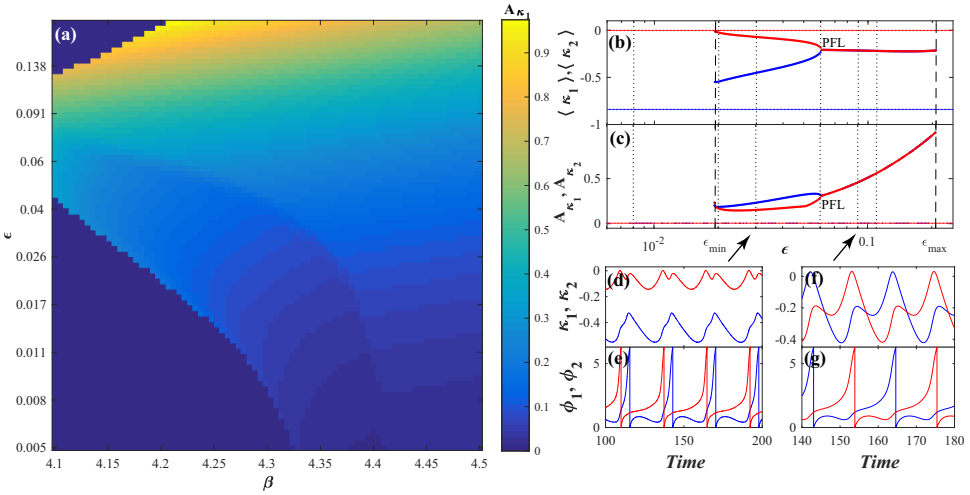

Fig. 3. Onset of oscillations in the full system (1) for $D = 0$. In panel (a) is shown how the variation A_{κ_1} of coupling weight κ_1 changes in the (β, ϵ) plane. Panel (b) shows how the mean coupling weights $\langle \kappa_1 \rangle$ and $\langle \kappa_2 \rangle$ of oscillatory states (thick lines) change with ϵ under fixed $\beta = 4.212$. The thin solid lines indicate the stationary state. In panel (c) are plotted the analogous dependencies for variation of the oscillation. The dotted lines in (b) and (c) indicate the ϵ values corresponding to the time traces in Figure 7, whereas the dashed lines indicate the boundaries of the ϵ region supporting the stable periodic solutions. The symmetry-breaking pitchfork bifurcation of limit cycles is denoted by PFL. In panels (d)–(g) are shown the waveforms of periodic solutions without and with the anti-phase space-time symmetry, obtained for $\epsilon = 0.03$ and $\epsilon = 0.09$, respectively (see the arrows). The excitability parameter is fixed to $I_0 = 0.95$.

4.1 Dynamics of the fast flow

Within the layer problem, one studies the dynamics of the fast variables

$$\begin{aligned} \dot{\varphi_1} &= I_0 - \sin\varphi_1 + \kappa_1 \sin(\varphi_2 - \varphi_1) \\ \dot{\varphi_2} &= I_0 - \sin\varphi_2 + \kappa_2 \sin(\varphi_1 - \varphi_2), \end{aligned} \tag{4}$$

where $\kappa_1, \kappa_2 \in [-1, 1]$ are considered as additional system parameters. Formally, system (4) is obtained by setting $\varepsilon = 0$ in (1) for $D = 0$.

The numerically obtained bifurcation diagram in Figure 4a shows that the fast flow is monostable for most of the (κ_1, κ_2) values, possessing either an equilibrium or a limit cycle attractor. The stability boundary of the periodic solution (red curves) has been obtained by the method of numerical continuation where, beginning from a stable periodic solution, the initial conditions for incremented parameter values are given by the final state reached for the previous set of (β, ϵ) values. The coexistence between a stable fixed point, lying on the synchronization manifold, and a limit cycle is found within a small region near the diagonal, see Figure 4a. Let us first classify the fixed points of the fast flow and then examine the scenarios that give rise to oscillations.

It can be shown that the fast flow admits either two or four fixed points, with the associated regions indicated in Figure 4b. In particular, two fixed points FP1 and FP2 on the synchronization manifold are *independent* on κ_1 and κ_2. They are given by $(\varphi_1^*, \varphi_2^*) = (\arcsin I_0, \arcsin I_0)$ and $(\varphi_1^*, \varphi_2^*) = (\pi - \arcsin I_0, \pi - \arcsin I_0)$. One may also find two additional fixed points off the synchronization manifold, referred

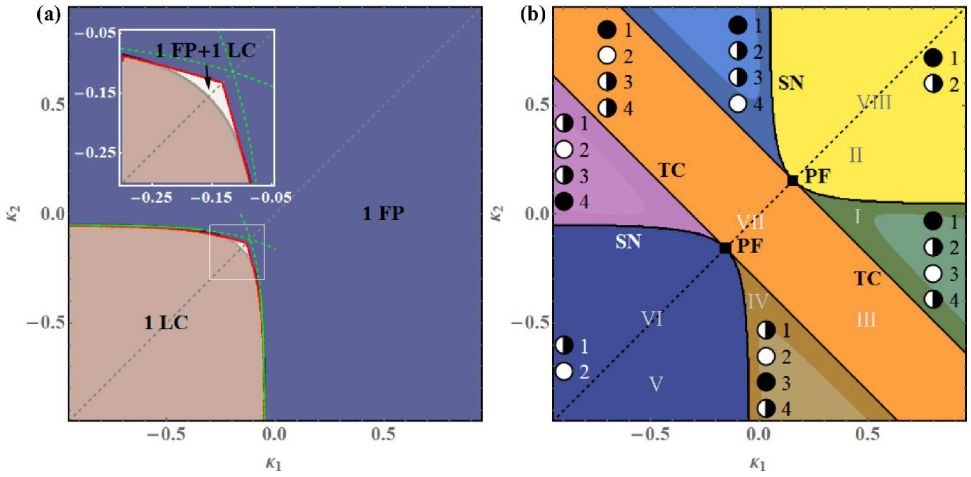

Fig. 4. (a) Attractors of the fast flow (4) in terms of κ_1 and κ_2, now considered as parameters. The fast flow is typically monostable, supporting either a stable fixed point (FP) or a stable limit cycle (LC), apart from a small region around the main diagonal, where it exhibits bistable behavior. The green dashed curves indicate approximations of two branches of SNIPER bifurcations, obtained by the method described in the text. The red lines correspond to the numerically determined stability boundaries of the oscillatory solution. (b) Classification of the fixed points of the fast flow (4). The fixed points are labeled the same way as in the main text, with their stability indicated as follows: full circles denote stable fixed points, semi-full circles represent saddle points and white circles correspond to doubly unstable fixed points. Within the four light-shaded triangular-shaped regions, the doubly unstable fixed point is a focus, rather than a node. The notation I–VIII refers to parameter values corresponding to the phase portraits in Figure 5.

to as FP3 and FP4 in Figure 4b. The bifurcations affecting the number and stability of the fixed points, beginning from the lower left region of the (κ_1, κ_2) plane, can be summarized as follows. Along the main diagonal $\kappa_1 = \kappa_2$, we find two points of supercritical pitchfork bifurcations (PF), where from the symmetric fixed points the saddles FP3 and FP4 appear and disappear. Off the main diagonal, the pitchforks are unfolded into curves of saddle-node (SN) and transcritical bifurcations (TC), see Figure 4b.

The (κ_1, κ_2) region featuring stable oscillations almost completely matches the lower left domain admitting two unstable fixed points. Within this region, each periodic solution obtained for (κ_1, κ_2) above the main diagonal $\kappa_1 = \kappa_2$ has a counterpart in the domain below the main diagonal, related to it by the exchange symmetry of units indices. Typically, the periodic solutions emerge via SNIPER bifurcations, comprising two branches where either κ_1 or κ_2 remain almost constant and close to zero. In both cases, the two fixed points that collide and disappear are FP3 and FP4. Nevertheless, such scenarios cannot be maintained in the small (κ_1, κ_2) region admitting coexistence between a fixed point and a limit cycle, because the SNIPER bifurcation is accompanied by a change in the number of fixed points. Our findings suggest that near the main diagonal, the limit cycle emerges via a heteroclinic bifurcation, where an orbit connects two saddles lying off the synchronization manifold (not shown). Note that the orbit of the limit cycle follows the unstable manifold of the saddle point FP2 on the synchronization manifold. To the left or the right of the main diagonal, instead of a heteroclinic bifurcation, one finds homoclinic bifurcations, whereby a saddle point, either FP3 or FP4, touches the limit cycle orbit. The schematic phase portraits indicating the stable and unstable manifolds of the fixed points and the limit

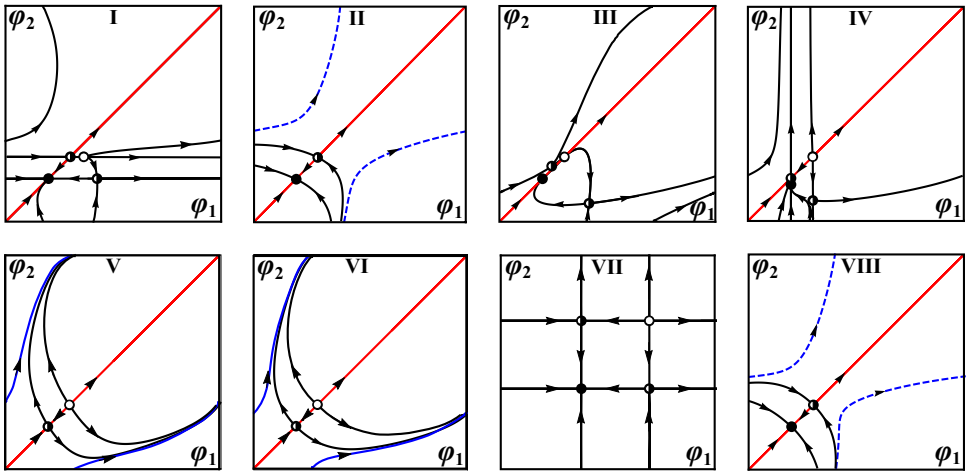

Fig. 5. Schematic phase portraits corresponding to the characteristic regimes of the fast flow. The panels I–VIII refer to representative parameter values indicated in Figure 4b. Also, the stability of fixed points is presented the same way as in Figure 4b. The invariant synchronization manifold is denoted by the red color, whereas the orbit of a stable/unstable limit cycle is indicated by the solid/dashed blue lines.

cycle for the characteristic regimes of the fast flow, denoted by I–VIII in Figure 4b, are illustrated in Figure 5.

The two branches of SNIPER bifurcations may readily be approximated for small values of κ_1 and κ_2 by a simple scheme, which amounts to reducing the fast flow to a normal form of saddle-node bifurcation. Suppose first that $\kappa_1 \ll 1$ and $I_0 - 1 \ll 1$. More specifically, let $\xi \ll 1$ be a small parameter such that $I_0 - 1 = \xi$ (close to the threshold) and $\kappa_1 = \gamma\xi$, i.e. γ is a rescaling parameter of κ_1, allowing for a zoom in the neighborhood of zero. Then, the steady states are given by the system

$$\begin{aligned} 1 + \xi - \sin\varphi_1 + \xi\gamma\sin(\varphi_2 - \varphi_1) &= 0, \\ 1 + \xi - \sin\varphi_2 + \kappa_2\sin(\varphi_1 - \varphi_2) &= 0. \end{aligned} \tag{5}$$

The first equation in the zeroth order approximation leads to $\varphi_1 = \pi/2$. Hence, using the perturbation approach, we have

$$\varphi_1^* = \frac{\pi}{2} + \sqrt{\xi}\Psi_1 + \cdots; \quad \varphi_2^* = \Psi_2 + \cdots, \tag{6}$$

where the $\sqrt{\xi}$ scaling follows from the Taylor expansion of the function $\sin\varphi_1$ at $\pi/2$. Inserting (6) into (5), one obtains the system of equations for Ψ_1 and Ψ_2

$$\begin{aligned} 1 + \frac{1}{2}\Psi_1^2 - \gamma\cos\Psi_2 &= 0, \\ 1 - \sin\Psi_2 + \kappa_2\cos\Psi_2 &= 0. \end{aligned} \tag{7}$$

From system (7), it is not difficult to see that the saddle-node bifurcation takes place if the condition $1 - \gamma\cos\Psi_2 = 0$ is satisfied. This leads to the parametric representation $\kappa_1 = \xi\gamma = \frac{I_0 - 1}{\cos\Psi_2}, \kappa_2 = \frac{\sin\Psi_2 - 1}{\cos\Psi_2}$, of the saddle-node curve for small κ_1 values, where Ψ_2 plays the role of the parameter along the curve. An analogous approach may be used to capture the second branch of saddle-node bifurcations, cf. the green dashed lines in Figure 4a.

4.2 Dynamics of the slow flow

We have numerically obtained the dynamics of the slow flow by applying a two-step approach. First, for fixed values (κ_1, κ_2), we determine the time-averaged dynamics of the fast flow (4), $\langle \varphi_2 - \varphi_1 \rangle_t = f(\kappa_1, \kappa_2)$. Here, the averaging $\langle \cdot \rangle_t$ is performed over a sufficiently large time interval, having eliminated a transient. Hence, this average depends on the attractor of the fast flow for the given (κ_1, κ_2). In particular, if the fast flow possesses a stable fixed point, then $\langle \varphi_2 - \varphi_1 \rangle_t = \varphi_2^* - \varphi_1^*$, where $(\varphi_1^*, \varphi_2^*)$ is a solution of

$$\begin{aligned} I_0 - \sin \varphi_1^* + \kappa_1 \sin(\varphi_2^* - \varphi_1^*) &= 0 \\ I_0 - \sin \varphi_2^* + \kappa_2 \sin(\varphi_1^* - \varphi_2^*) &= 0. \end{aligned} \tag{8}$$

This procedure just results in determining the slow critical manifold of the system. In case when the attractor of the fast flow is periodic, $\langle \varphi_2 - \varphi_1 \rangle_t$ presents the time average over the period. Averaging approximation in case of a periodic attractor of the fast flow constitutes a standard approach [13,25], rather natural for describing the influence of oscillations in the fast flow on the dynamics of the slow flow. At the second stage, the obtained time-averages are substituted into the dynamics of the weights

$$\begin{aligned} \dot{\kappa_1} &= \epsilon[-\kappa_1 + \sin(f(\kappa_1, \kappa_2) + \beta)] \\ \dot{\kappa_2} &= \epsilon[-\kappa_2 + \sin(-f(\kappa_1, \kappa_2) + \beta)]. \end{aligned} \tag{9}$$

The system (9) is used to determine the vector field of the slow flow by taking into account only the attractors of the fast flow, such that the vector field associated to each attractor is plotted within its respective stability region, cf. Figure 6.

In regions of the (κ_1, κ_2) plane where there are coexisting stable solutions of the fast flow, the corresponding vector field of the slow flow is given on multiple overlapping sheets, since the value of the average $f(\kappa_1, \kappa_2)$ depends on the initial conditions. In our case, this occurs only in a small region of coexistence between an equilibrium and a stable limit cycle.

One should single out two important features of the slow flow: (i) it exhibits two symmetry-related fixed points in the green and blue regions in Figure 6, and (ii) the slow vector field is pointed in opposite directions close to the boundary between the fast oscillatory regime (orange region) and the steady states of the fast flow (blue, green and white regions). The latter in particular implies that interesting effects occur close to the border of the oscillatory and the steady state regime of the fast flow. Moreover, adding noise gives rise to fluctuations around this boundary, which leads to switching between the quasi-stationary and the fast spiking dynamics. Such effects are studied in more detail within the next section.

5 Switching dynamics

Our main observation in this section is that the interplay of plasticity and noise induces slow stochastic fluctuations (switching dynamics), mediating two qualitatively different scenarios depending on the speed of adaptation. The latter include (i) switching between two modes of *noise-induced* oscillations for slower adaptation (small $\epsilon \simeq 0.01$) and (ii) switching between multiple coexisting attractors of the deterministic dynamics for faster adaptation (intermediate $\epsilon \simeq 0.05$).

In case (i), the impact of noise is twofold: on a short timescale, it gives rise to spiking dynamics, whereas on a long time scale, it induces random transitions between

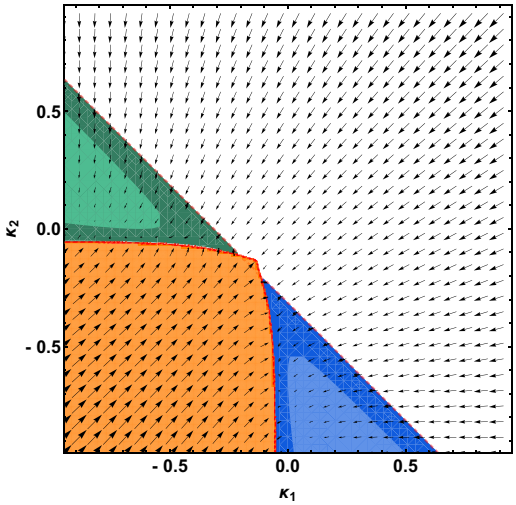

Fig. 6. Vector field of the slow flow obtained by taking into account only stable attractors of the fast flow for $\beta = 4.212, I_0 = 0.95$. The color coding is as follows: orange color denotes the region associated to the stable limit cycle of the fast flow, white stands for the stable fixed point of the fast flow FP1, whereas blue and green color correspond to the two stable fixed points FP3 and FP4. Within the light-shaded regions, FP3 and FP4 are foci rather than nodes, cf. Figure 4b.

the two oscillatory modes. In case (ii), the switching dynamics comprises metastable states derived from two fixed points, as well as two limit cycles associated to emergent oscillations of the corresponding deterministic system. The key difference between the effects (i) and (ii) is that for slower adaptation, the system switches between the oscillatory modes that do not exist as deterministic attractors. Moreover, the two generic types of switching are characterized by distinct phase dynamics: for slower adaptation, one finds alternation of patterns with different order of spiking between the units, whereas for faster adaptation, the phases effectively exhibit bursting behavior, involving a succession between episodes of spiking and relative quiescence. An overview on how the typical dynamics of couplings changes with ϵ at fixed β is provided in Figure 7. Note that the difference between the average coupling weights of the stable periodic solutions of the deterministic system are much smaller than a typical distance between the coupling levels for the stationary states. The prevalence of metastable states is affected by ϵ so that intermediate adaptation favors oscillatory modes, whereas the fast adaptation apparently promotes the two quasi-stationary states. In the next two subsections, we provide further insight into the mechanisms behind the switching dynamics using the results of the fast-slow analysis.

5.1 Switching dynamics under slow adaptation

As already indicated, ϵ is here taken sufficiently small, such that it cannot facilitate emergent oscillations in the full system (1). For $\epsilon \simeq 0.01$ and under appropriate noise levels, one observes noise-induced oscillations [26]. The latter arise via a scenario involving a multiple-timescale stochastic bifurcation, whereby noise acts only within the fast subsystem of (1). The onset of oscillations under increasing D occurs in two stages. In the first stage, the phase dynamics gradually exhibits more induced spikes,

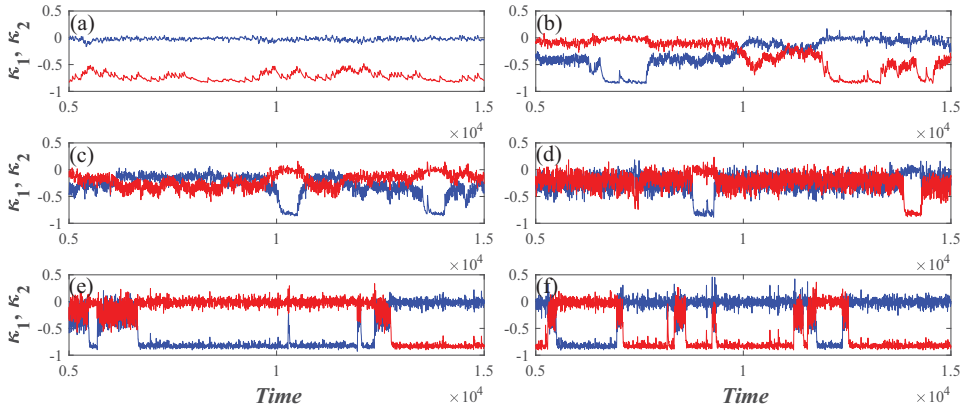

Fig. 7. Switching dynamics under variation of ϵ. The time traces $(\kappa_1(t), \kappa_2(t))$ are obtained for fixed $I_0 = 0.95$, $D = 0.006$, $\beta = 4.212$, whereas ϵ assumes the following values: (a) $\epsilon = 0.008$, (b) $\epsilon = 0.02$, (c) $\epsilon = 0.03$, (d) $\epsilon = 0.06$, (e) $\epsilon = 0.09$, (f) $\epsilon = 0.11$.

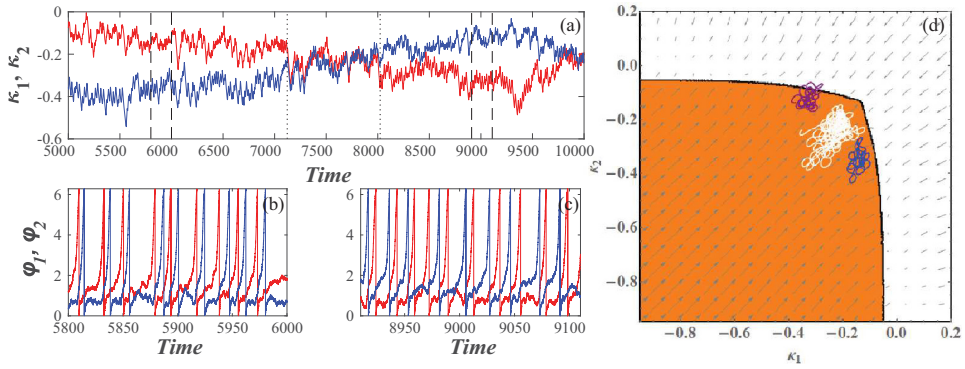

Fig. 8. Switching dynamics between the two modes of noise-induced oscillations. Time traces of the weights are shown in panel (a), whereas panel (b) and (c) display the corresponding time traces of the phases during the intervals between the dashed lines in panel (a). In panel (d), the $(\kappa_1(t), \kappa_2(t))$ projections of the orbits associated to each of the two modes (blue color), as well as the switching episode, shown in white, are superimposed to the vector field of the slow flow from Figure 6. The shaded area corresponds to the stable limit cycle. The system parameters are $I_0 = 0.95, \beta = 4.212, \epsilon = 0.01, D = 0.009$.

such that the stationary distributions of phases eventually acquire a longer tail reflecting the occurrence of spikes (not shown). Nevertheless, the stationary distributions $P(\kappa_i)$ change appreciably only at the second stage, which takes place for sufficiently large D. Such a change accompanies the emergence of coupling oscillations. Note that the system (1) actually exhibits *two modes* of noise-induced oscillations, characterized by the different order of firing between the two units, cf. the time traces of phase dynamics and the associated evolution of couplings in Figure 8a.

It is interesting to examine whether the vector field of the slow flow from Section 4.2 can be used to explain the slow stochastic fluctuations of the coupling weights. To this end, we have superimposed the $(\kappa_1(t), \kappa_2(t))$ orbits of the two noise-induced modes, as well as a switching episode, to a vector field of the slow flow from Figure 6. Note that the orbits typically lie close to the boundary outlining the transition between the two attractors of the fast flow, featuring non-negligible coupling weights. Moreover, the two modes are confined to small areas of the (κ_1, κ_2) plane

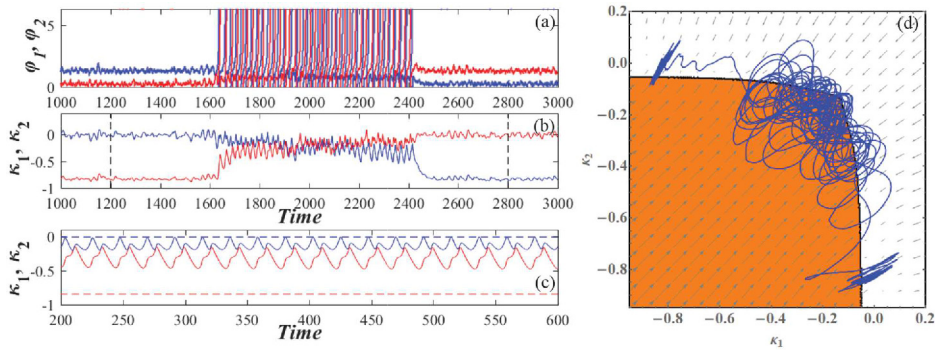

Fig. 9. Time traces of the phases (a) and weights (b) associated to noise-induced switching between the coexisting attractors of the deterministic system. The results are obtained for $I_0 = 0.95, \beta = 4.212, \epsilon = 0.05, D = 0.004$. In panel (c) is provided the deterministic dynamics of weights obtained for the same parameter values. In panel (d), the $(\kappa_1(t), \kappa_2(t))$ orbit corresponding to the interval between the dashed lines in (b) is super-imposed on the vector field of the slow flow cf. Figure 6.

symmetrical with respect to the main diagonal $\kappa_1 = \kappa_2$, whereas the switching episode virtually takes place on the diagonal. Apparently, the noise-induced modes occupy regions where the oscillations in the fast flow emerge via homoclinic bifurcations, rather than the SNIPER scenario. Nonetheless, the switching episode seems to involve the domain featuring coexistence of the two stable sheets of the slow vector field. Within these sheets, which correspond to two attractors of the fast flow (a stable node and a stable limit cycle), the vector fields are oriented in opposite directions, thereby contributing to switching.

5.2 Switching dynamics for faster adaptation

In case of faster adaptation associated to intermediate ϵ, the switching dynamics involves four metastable states, derived from the attractors of the deterministic system. The deterministic multistable behavior includes two symmetry-related stationary states, as well as two symmetry-related limit cycles. Note that while the two stable steady states exist for arbitrary small ϵ and are therefore visible in the slow flow in Figure 6, the oscillatory solutions disappear for small ϵ and hence cannot be observed in the slow flow. The two oscillatory regimes are characterized by the same phase shift, but the reverse order of firing between the two units. Influenced by noise, the phases effectively engage in bursting behavior, manifesting slow stochastic fluctuations between episodes of intensive spiking activity and periods of relative quiescence, see Figure 9a. For a fixed noise level, the prevalence of metastable states, defined by transition probabilities between them, changes with adaptation speed. One observes that for $\epsilon \simeq 0.05$, the oscillatory dynamics is preferred, whereas for $\epsilon \simeq 0.1$, the quasi-stationary states are more ubiquitous.

A comparison of the (κ_1, κ_2) orbits displaying switching dynamics and the vector field of the slow flow from Figure 6 again shows that the former is confined to the criticality region at the boundary between the stationary and oscillatory regimes in the fast flow, cf. Figure 9. One should remark on how the transitions between the different metastable states take place. In particular, from Figure 9b, it is clear that there can be no direct transitions between the two quasi-stationary states, but they rather have to be mediated by the system passing through the oscillatory states. Also, the transition from oscillatory to quasi-stationary states typically occurs

once the couplings approach a master-slave-like configuration, where the coupling in one direction is much stronger than the other one. This scenario coincides with the SNIPER bifurcation of the fast flow described in Section 4.1. The scenario of transition between the two metastable oscillatory states resembles closely the one from Section 5.2.

6 Summary

In the present study, we have analyzed a system of two adaptively coupled active rotators with excitable intrinsic dynamics, demonstrating that the interplay of plasticity and noise may give rise to slow stochastic fluctuations. Two qualitatively different types of self-organized behavior have been identified, depending on the adaptation speed. For slower adaptation, the switching dynamics consists of an alternation between two modes of noise-induced oscillations, associated to a preferred order of spiking between the two units. In this case, noise plays a twofold role: on one hand, it perturbs the excitable local dynamics giving rise to oscillations on a short timescale, whereas on the other hand, it elicits the alternation between the two oscillatory states on a long timescale. The underlying phase dynamics shows slow switching between two patterns distinguished by the different order in which the units are spiking. In case of faster adaptation, the coupling becomes capable of eliciting emergent oscillations in the deterministic system [27]. The latter then exhibits complex multistable behavior, involving two stationary and two oscillatory regimes. Under the influence of noise, the system undergoes switching between these four different metastable states, whose prevalence at fixed noise level depends on the speed of adaptation. The deterministic attractors associated to metastable states are related by the Z_2 symmetry. Thus, a mismatch in excitability parameters would lead to symmetry-breaking, whereby a small mismatch would induce a bias in switching dynamics, whereas a larger mismatch, corresponding to a scenario with one excitable and one oscillatory unit, would completely alter the observed dynamics.

Though the underlying phenomena are not found in the singular limit of infinite scale separation, the fast-slow analysis we have applied still allows one to explain the qualitative features of both considered types of switching behavior. Studying the layer problem, and in particular the vector field of the slow flow, has enabled us to gain insight into the metastable states and the transitions between them. It has been demonstrated that the coupling dynamics is always in a state of "criticality", being confined to the boundary between the stationary and oscillatory regimes of the fast flow.

Given that excitability, plasticity and noise are inherent ingredients of neuronal systems, the obtained results can be interpreted in the context of neuroscience. It is well known that the backbone of neural networks is made up of binary and ternary neuron motifs, whereby the structural motifs typically support multiple functional motifs, essentially characterized by the weight configuration and the underlying direction of the information flow. With this in mind, the scenario of switching under slow adaptation may be important, because it implies that a binary motif can display slow alternation between two effectively unidirectional weight configurations, promoting opposite direction of information flow. For faster adaptation, one finds multistability between unidirectional coupling and bidirectional coupling of moderate strength. Nonetheless, the underlying phase dynamics, if extended to networks, may be considered as a paradigm for UP-DOWN states, typical for cortical dynamics [28,29]. Thus, it would be of interest to examine the impact of plasticity in networks of noisy excitable units, where one may expect different types of emergent behavior, such as cluster, non-synchronized and partially synchronized states, depending on the frustration of local dynamics and the impact of noise.

We thank S. Eydam for useful discussions. This work was supported by the Ministry of Education, Science and Technological Development of Republic of Serbia under project No. 171017, the DAAD Serbia-Germany Bilateral Project "Emergent Dynamics in Systems of Coupled Excitable Units", as well as the DFG within the framework of Collaborative Research Center SFB 910.

Author contribution statement

I.F. and S.Y. conceived the model and defined the analysis of noise-induced switching as the main goal of the research. S.Y. and M.W. developed the general framework to investigating the deterministic fast-slow problem and the bifurcation analysis of the associated reduced systems. I.B. obtained all the numerical results, whereas I.B. and I.F. carried out the bifurcation analysis, identified the two types of noise-induced switching behavior and made the main contribution to writing the manuscript. All the authors discussed the findings and participated in interpretation of the results.

References

1. F. Sorrentino, E. Ott, Phys. Rev. Lett. **100**, 114101 (2008)
2. F. Vazquez, V.M. Eguiluz, M.S. Miguel, Phys. Rev. Lett. **100**, 108702 (2008)
3. N. Caporale, Y. Dan, Ann. Rev. Neurosci. **31**, 25 (2008)
4. C. Furusawa, K. Kaneko, Phys. Rev. Lett. **90**, 088102 (2003)
5. D.O. Hebb, *The Organization of Behavior: a Neuropsychological Approach* (John Wiley & Sons, New York, 1949)
6. S. Song, K.D. Miller, L.F. Abbott, Nat. Neurosci. **3**, 919 (2000)
7. R.C. Froemke, Y. Dan, Nature (London) **416**, 433 (2002)
8. H.-X. Wang, R.C. Gerkin, D.W. Nauen, G.-Q. Bi, Nat. Neurosci. **8**, 187 (2005)
9. O. Sporns, R. Kotter, PLoS Biol. **2**, e369 (2004)
10. I. Franović, V. Miljković, Chaos Soliton. Fract. **44**, 122 (2011)
11. I. Franović, V. Miljković, Chaos Soliton. Fract. **45**, 527 (2012)
12. I. Franović, V. Miljković, EPL **92**, 68007 (2011)
13. L. Lücken, O.V. Popovych, P.A. Tass, S. Yanchuk, Phys. Rev. E **93**, 032210 (2016)
14. Y.L. Maistrenko, B. Lysyansky, C. Hauptmann, O. Burylko, P.A. Tass, Phys. Rev. E **75**, 066207 (2007)
15. P. Seliger, S.C. Young, L.S. Tsimring, Phys. Rev. E **65**, 041906 (2002)
16. M. Li, S. Guan, C.-H. Lai, New J. Phys. **12**, 103032 (2010)
17. P.S. Skardal, D. Taylor, J.G. Restrepo, Physica D **267**, 27 (2014)
18. D. Kasatkin, S. Yanchuk, E. Schöll, V. Nekorkin, Phys. Rev. E **96**, 062211 (2017)
19. O.V. Popovych, S. Yanchuk, P.A. Tass, Sci. Rep. **3**, 2926 (2013)
20. K. Mikkelsen, A. Imparato, A. Torcini, Phys. Rev. Lett. **110**, 208101 (2013)
21. D. Millman, S. Mihalas, A. Kirkwood, E. Niebur, Nat. Phys. **6**, 801 (2010)
22. A. Levina, J.M. Hermann, T. Geisel, Phys. Rev. Lett. **102**, 118110 (2009)
23. T. Aoki, T. Aoyagi, Phys. Rev. Lett. **102**, 034101 (2009)
24. T. Aoki, T. Aoyagi, Phys. Rev. E **84**, 066109 (2011)
25. A. Shilnikov, Int. J. Bifurc. Chaos **18**, 2141 (2008)
26. S.-J. Wang, G. Ouyang, J. Guang, M. Zhang, Phys. Rev. Lett. **116**, 018101 (2016)
27. Q. Ren, K.M. Kolwankar, A. Samal, J. Jost, Phys. Rev. E **86**, 056103 (2012)
28. T.T.G. Hahn, J.M. McFarland, S. Berberich, B. Sakmann, M.R. Mehta, Nat. Neurosci. **15**, 1531 (2012)
29. V.V. Vyazovskiy, K.D. Harris, Nat. Rev. Neurosci. **14**, 443 (2013)